nanomaterials

Article

Synthesis of CaF_2 Nanoparticles Coated by SiO_2 for Improved Al_2O_3/TiC Self-Lubricating Ceramic Composites

Zhaoqiang Chen [1,2,*], Niansheng Guo [1,2], Lianggang Ji [1,2] and Chonghai Xu [1,2]

1 School of Mechanical and Automotive Engineering, Qilu University of Technology (Shandong Academy of Sciences), Jinan 250353, China; G1758251323@163.com (N.G.); jilianggang123@126.com (L.J.); xch@qlu.edu.cn (C.X.)
2 Key Laboratory of Advanced Manufacturing and Measurement and Control Technology for Light Industry in Universities of Shandong, Qilu University of Technology (Shandong Academy of Sciences), Jinan 250353, China
* Correspondence: czq@qlu.edu.cn

Received: 26 September 2019; Accepted: 22 October 2019; Published: 25 October 2019

Abstract: In order to reduce the influence of CaF_2 addition on the mechanical properties of self-lubricating ceramic tools, we applied a silicon dioxide (SiO_2) coating on calcium fluoride (CaF_2) nanoparticles through hydrolysis and condensation reactions using the tetraethoxysilane (TEOS) method. The powder was dried by the azeotropic method, so that it acquired a better dispersibility. The resulting composite powders were characterized using XRD (X-ray diffraction) and TEM (transmission electron microscopy), showing that the surface of CaF_2 was coated with a layer of uniform and compact SiO_2. SiO_2 shells with different thicknesses could be obtained by changing the amount of TEOS added, and the thickness of the SiO_2 shells could be controlled between 1.5 and 15 nm. At the same time, a ceramic material containing CaF_2 nanoparticles and CaF_2@SiO_2-coated nanoparticles was prepared. It had the best mechanical properties when CaF_2@SiO_2-coated nanoparticles were added; its flexural strength, fracture toughness, and hardness were 562 ± 28 MPa, 5.51 ± 0.26 MPa·$m^{1/2}$, and 15.26 ± 0.16 GPa, respectively. Compared with the ceramic tool containing CaF_2 nanoparticles, these mechanical properties were increased by 17.57%, 12.67%, and 4.88%, respectively. The addition of CaF_2@SiO_2-coated nanoparticles greatly improved the antifriction and wear resistance of the ceramic material, and the antifriction and wear resistance were balanced.

Keywords: SiO_2-coated CaF_2; solid lubricant; self-lubricating ceramic tool; nanoparticles

1. Introduction

Calcium fluoride (CaF_2) crystals have good optical properties, mechanical properties, and chemical stability; therefore, calcium fluoride is widely used [1–5]. Calcium fluoride crystals are very important optical functional crystals, which have the advantages of wide light transmission range, high transmittance, low refractive index, low dispersion, and so on and have become an irreplaceable lens material in ultraviolet lithography objective lens systems [6–9]. At the same time, calcium fluoride has low shear strength and thermophysical and thermochemical stability at high temperature, so it is used in high-temperature solid lubrication [10–14]. At present, calcium fluoride has been applied in the field of self-lubricating ceramics allowing made some advances [15–20]. Wu et al. [17] prepared an Al_2O_3/TiC/CaF_2 multicomponent gradient self-lubricating ceramic composite by the hot-pressing method, showing that the addition of CaF_2 could improve the antifriction properties of the ceramic composite. In the work by Kong et al. [21], a ZrO_2–MoS_2–CaF_2 self-lubricating composite was prepared.

A ZrO_2 matrix composite showed a good tribological behavior over a wide temperature range with the addition of MoS_2 and CaF_2. On the one hand, the addition of calcium fluoride to self-lubricating ceramic materials will improve the wear resistance of the materials, while, on the other hand, it will reduce the mechanical properties of the materials and the overall reliability of the ceramic tool. One of the main problems to be solved is how to maintain high mechanical properties of self-lubricating ceramic tools together with high lubricating performance.

With the development of nanotechnology, the properties of nanomaterials, such as small size effect and macroscopic quantum-tunneling effect, have been attracted more and more attention. In particular, preparation and applications of nano-calcium fluoride have been greatly developed [22–25]. The introduction of nano-materials can improve the mechanical properties as well as the friction and wear properties of composite ceramic materials [26–30]. At the same time, because nanoparticles have high surface energy and chemical activity, they can be easily deposited on a worn surface during the friction process, forming a protective layer with low melting point and easy shearing and thus playing a good anti-friction and anti-wear role [31–34]. However, nano-materials have the problems of small particle size, large specific surface area, and high surface activity, which make nano-materials easy to agglomerate, thus affecting their performance [35,36]. Powder coating refers to the process of adsorbing or coating another substance or substances on the surface of a powder to form a composite material with a core–shell structure. Powder coating can change the physical and chemical properties of a powder [37–44]. Hu et al. [41] successfully coated SiO_2 on the surface of monodisperse $CoFe_2O_4$, proving that the silica coating can prevent the aggregation and growth of nanoparticles at high temperature, making the nanoparticles suitable for various high-temperature technological applications. Wu et al. [42] prepared h-BN@Ni powders, which, compared to h-BN powders, greatly improved the mechanical properties of self-lubricating tools. In the work by Zhang et al. [43], a core–shell nanocomposite with polytetrafluoroethylene as the core and polymethyl methacrylate as the shell was prepared. The mechanical and lubricating properties of the nanocomposite were significantly improved.

In self-lubricating ceramic tools, the direct addition of calcium fluoride will significantly reduce the mechanical properties of the cutting tools, because the mechanical properties of calcium fluoride are relatively low [17,19]. Therefore, core–shell coating of calcium fluoride has been used to maintain simultaneously high mechanical properties and lubricity of the cutting tools [45]. In this paper, a layer of silicon dioxide was successfully coated on the surface of CaF_2 nanoparticles through hydrolysis and condensation reactions with the tetraethoxysilane (TEOS) method. The powder coating was combined with nano powder, and the $CaF_2@SiO_2$-coated nanoparticles were added to replace CaF_2 nanoparticles in the self-lubricating ceramic tool. The mechanical properties and the wear resistance of the ceramic tool were greatly improved, and the ceramic tool had antifriction properties.

2. Experimental Procedure

2.1. Materials and Processing

The starting materials used to prepare the $CaF_2@SiO_2$-coated nanoparticles are commercially available: $Ca(NO_3)_2$ (purity > 99.9%, Shanghai Fine Chemical Co., Ltd., Shanghai, China), NH_4F (analytically pure, Tianjin Chemical Reagent Factory, Tianjin, China), NH_3H_2O (analytically pure, Tianjin Chemical Reagent Factory, Tianjin, China), TEOS analytical reagent (Tianjin Botong Chemical Co., Ltd., Tianjin, China), n-butanol, distilled water, and absolute ethanol were used as received without further purification.

2.2. Synthesis of $CaF_2@SiO_2$ Powders

According to the molar ratio of 1:1.5, calcium nitrate and ammonium fluoride were weighed and dissolved in equal volumes of absolute ethyl alcohol and water, respectively, and stirred until completely dissolved; then, an absolute ethyl alcohol solution containing polyethylene glycol (PEG) was added, and ultrasonic dispersion and mechanical stirring were carried out for 20 min to uniformly disperse the calcium nitrate and ammonium fluoride. A calcium nitrate dispersion was slowly added into the ammonium fluoride dispersion through a constant-pressure separatory funnel, and ultrasonic stirring was continuously carried out during the process. After reacting for 30 min, the mixture was left standing for 2 h. The obtained product was centrifuged for 30 min at 4000 r/min, washed with distilled water for 3 times, and azeotropically dried to obtain a nano-calcium fluoride powder. Then, 1 g of self-made nano-CaF_2 powder was weighed, and 100 mL of absolute ethyl alcohol solution and a proper amount of dispersant polyvinylpyrrolidone (PVP) were added, followed by ultrasonic dispersion for 40 min and heating in a water bath under rapid stirring, while keeping the temperature between 35 and 45 °C. Distilled water (2.5 mL) was added to the above solution, and the pH was adjusted to 8.5 by adding an appropriate amount of ammonia water. To the above mixed solution, 1–4 mL of TEOS was slowly added dropwise, after which the mixture was continuously heated and rapidly stirred for 1 h. The obtained suspension was centrifuged at 6000 r/min for 25 min, then washed with anhydrous ethanol for 3 times. After cleaning, a wet gel was added into a 6:4 solution of n-butanol and distilled water, and after ultrasonic stirring for 30 min, the powder was azeotropically dried to obtain the CaF_2@SiO_2 composite powder with nano-CaF_2 as core and SiO_2 as shell.

2.3. Preparation of the Self-Lubricating Ceramic Tool Materials

The purity of each raw particle was higher than 99.9%. The average particle size of each particle were as follows: Al_2O_3 powder, 0.5 µm, TiC, 0.5 µm, MgO, 1 µm; the average size of the core–shell solid lubricant composite particles CaF_2 made in our own laboratory was 30–50 nm.

The Al_2O_3/TiC/CaF_2@SiO_2 (ATCS) self-lubricating ceramic composite was prepared by the vacuum hot-pressing sintering technique. The sintering temperature was 1650 °C, the heating rate was 20 °C/min, the holding time was 20 min, and the hot-pressing pressure was 30 MPa. The volume ratio of commercially available, high-purity Al_2O_3 to TiC was 7:3, while the volume fraction of CaF_2@SiO_2 was 10%. For comparison, the Al_2O_3/TiC/CaF_2(ATC) self-lubricating ceramic composite was prepared under the same conditions.

2.4. Performance Testing of Tool Materials

The resulting ceramic embryo body obtained was processed into a standard sample with a size of 3 mm × 4 mm × 30 mm to test the mechanical properties of the material. A bending strength test was performed by a three-point bending method with a span of 20 mm and a displacement loading speed of 0.5 mm/min. Vickers hardness was measured by a Hv-120 Vickers hardness tester with an indentation load of 196 N and dwell time of 15 s. Fracture toughness was measured by the indentation method, and fracture toughness was determined by indentation crack length [42].

2.5. Characterization

X-ray diffraction (XRD, D8-ADVANCE, Bruker AXS Co., Karlsruhe, Germany) was used for phase identification of the CaF_2 nanoparticles and CaF_2@SiO_2-coated nanoparticles. X-ray diffraction was carried out using Cu Kα radiation with 40 kV and 40 mA, and the samples were analyzed at room temperature over a 2θ range from 15° to 80° and at a scanning rate of 10°/min. Morphology and crystallinity of the CaF_2 nanoparticles and CaF_2@SiO_2-coated nanoparticles were obtained by transmission electron microscopy (TEM, JEM-1400, JEOL, Tokyo, Japan). The fracture morphology of the ceramic tools was examined and analyzed using a field-emission scanning electron microscope (SEM, Regulus8220, HITACHI, Tokyo, Japan), along with an energy-dispersive spectroscope (EDS).

3. Results and Discussion

3.1. Characterization of Structure and Morphology

Figure 1 shows the XRD patterns of the as-prepared CaF_2@SiO_2 nanoparticles and pure CaF_2 nanoparticles. Figure 1a shows the XRD patterns of CaF_2 nanoparticles. All the discernible peaks were in good agreement with the data of pure cubic CaF_2 crystals (JCPDS NO.35–0816). The diffraction peak of CaF_2 crystals was narrow and sharp, which indicated that the prepared CaF_2 had high crystallinity, and no impurity peak was detected, indicating that the prepared CaF_2 had high purity. As shown in Figure 1b, the XRD patterns of CaF_2@SiO_2 nanoparticles were the same as the XRD patterns of pure cubic CaF_2 crystals; only at about 2θ = 20°–25°, the pattern for CaF_2@SiO_2 had a low and wide peak, attributed to a silica dioxide amorphous halo [37,41].

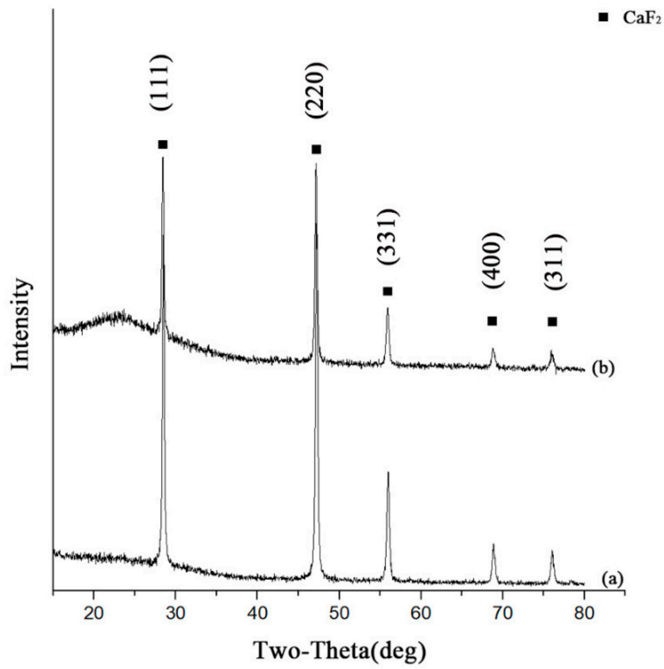

Figure 1. XRD patterns of (**a**) pure CaF_2 and (**b**) CaF_2@SiO_2.

The TEM images of the pure CaF_2 and CaF_2@SiO_2 nanoparticles are shown in Figure 2. Figure 2a shows a transmission electron microscope image of pure CaF_2. As shown in Figure 2a, the CaF_2 nanoparticles had good dispersibility and an approximately round flake structure, and the average particle size of nano CaF_2 was about 30–50 nm. Figure 2b shows a transmission electron microscope image of CaF_2@SiO_2 nanoparticles. The TEM micrograph clearly shows that the surface of the CaF_2 nanoparticles was covered by a layer of amorphous SiO_2, and the smooth edge of the CaF_2 was tightly covered by amorphous SiO_2. The coated powder had good dispersibility, and the average thickness of the amorphous silica coating was about 3.6 nm. The thickness of the SiO_2 shell in the coated CaF_2@SiO_2 nanoparticles can be regulated and controlled; it can be changed by varying the amount of TEOS added. Figure 3 is a high-resolution transmission electron microscopy (HRTEM) image of CaF_2@SiO_2-coated nanoparticles. The HRTEM image shows that the lattice fringes were about 0.319 nm, which corresponds to the (111) orientation of CaF_2. Amorphous SiO_2 was evenly coated on the edge of calcium fluoride, and SiO_2 and the CaF_2 tightly combined. This shows that SiO_2 was successfully coated on the surface of CaF_2 nanoparticles, providing a uniform coating and a good coating effect.

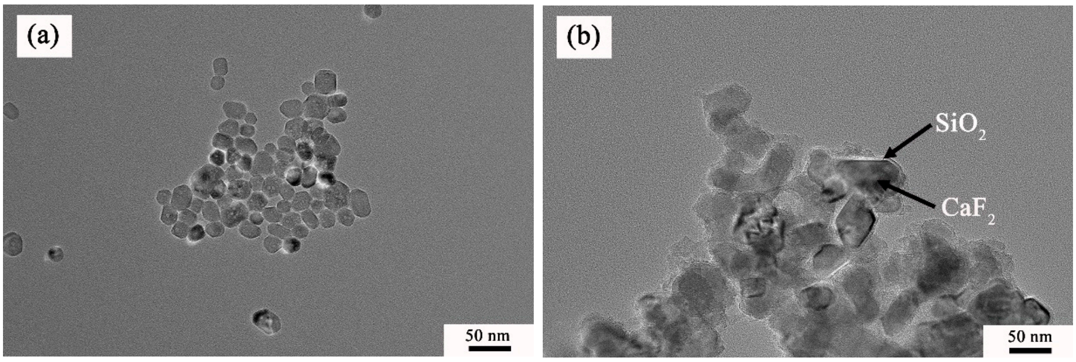

Figure 2. TEM micrographs of (**a**) CaF_2 and (**b**) CaF_2@SiO_2.

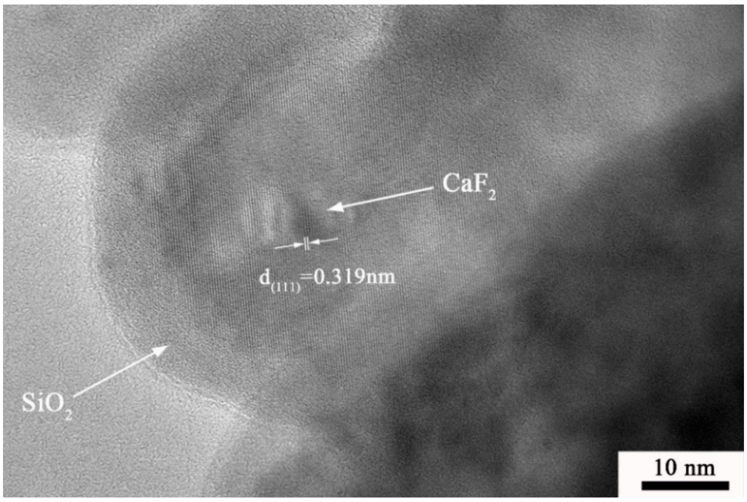

Figure 3. HRTEM micrographs of CaF_2@SiO_2.

3.2. Effect of TESO Addition on Coating Thickness

TEM images of CaF_2@SiO_2-coated powder with different amounts of TEOS are shown in Figure 4. The amount of CaF_2 was 1 g, the pH value was 8.5, and the amounts of TEOS were 1 mL, 2 mL, 3 mL, and 4 mL. The white framed images are partial enlarged views of the red selected areas. Figure 4a shows the powder obtained when 1 mL of TEOS was added; it can be seen from the figure that this TEOS amount resulted in less amorphous SiO_2. At the edge of nano CaF_2, the thickness of the SiO_2 shell was very small, about 1.2 nm. When the amount of TEOS added was increased to 2 mL (Figure 4b), the thickness of the SiO_2 shell coated on the nano-CaF_2 increased to about 3.6 nm, but the coating effect was poor, and the thickness of the SiO_2 shell was uneven. As shown in Figure 4c, when the amount of TEOS added was 3 mL, the thickness of the SiO_2 shell increased to about 5.8 nm. At the same time, it can be seen that the amorphous SiO_2 coated on CaF_2 had uniform thickness and a good coating effect, but slight agglomeration occurred. When the amount of TEOS further increased to 4 mL, the thickness of the SiO_2 shell reached about 13.3 nm, the coating thickness was relatively uniform, but agglomeration was more pronounced. The thickness of the SiO_2 shell coated on CaF_2 increased with the increase of the amount TEOS, but when the amount of TEOS added was too large, agglomeration occurred, whereas when the amount of TEOS was 3 mL, the best coating effect was obtained. SiO_2 shells with different thicknesses could be obtained by changing the amount of TEOS added, and the thickness of the SiO_2 shell could be controlled between 1.5 and 15 nm.

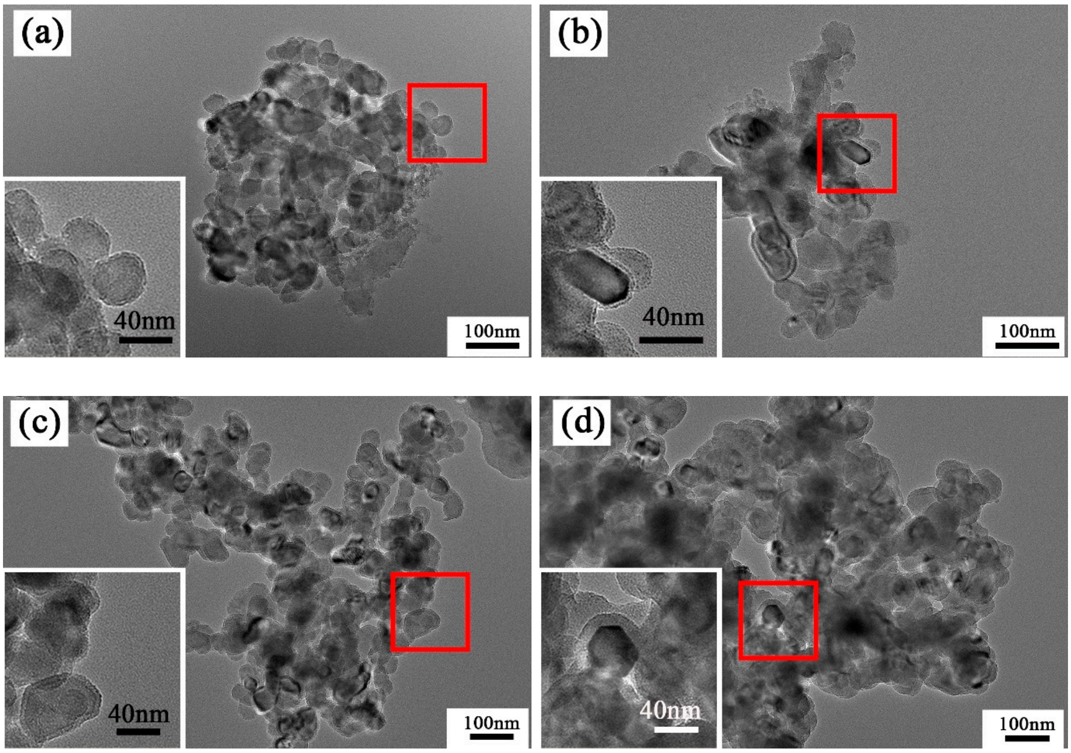

Figure 4. TEM micrographs in the presence of different tetraethoxysilane (TEOS) amounts. (**a**) 1 mL (**b**) 2 mL (**c**) 3 mL (**d**) 4 mL of TEOS.

3.3. Improvement in Mechanical Properties and Microstructurs

The scanning electron micrographs and EDS spectra of the fracture surfaces of the Al_2O_3/TiC/CaF_2 ceramic composite are shown in Figure 5. EDS analysis results showed that the larger crystal grains in the Figure 5 were alumina crystals. According to the distribution of the F element, it can be seen that a large amount of uniformly dispersed nano-calcium fluoride was distributed on the surface of the alumina crystal grains. From the SEM images of the fracture surfaces, it can be seen that fine white protrusions were uniformly distributed on the surface of the alumina grains. These white protrusions were self-made nano-calcium fluoride grains, which formed an in-crystal nanostructure. The fracture mode of the ceramic composites was mainly intergranular fracture, with a small amount of transgranular fracture.

The scanning electron micrographs and EDS spectra of the fracture surfaces of the Al_2O_3/TiC/CaF_2@SiO_2 ceramic composite are shown in Figure 6. EDS analysis results showed that Si elements were mostly distributed at the grain boundaries between the right-hand grains. From the SEM images of the fracture surfaces, it can be seen that the nano-CaF_2 protrusions on the surface of the alumina grains decreased, while the alumina grains became fine and the grain boundaries between the grains became blurred. Transgranular fracture increased, and intergranular fracture occurred in the ceramic composite. The fracture mode of the tools was mainly transgranular fracture. Transgranular fracture consumes a large amount of fracture energy, which is helpful to improve the mechanical properties of tool materials, making them compact with less defects. The addition of the coating powder plays a role in refining the crystal grains of a ceramic composite, improving the mechanical properties of the ceramic composite, enhancing the interfacial bonding force of the ceramic matrix material, changing the main fracture mode of the cutter, and improving the mechanical properties of the ceramic composite.

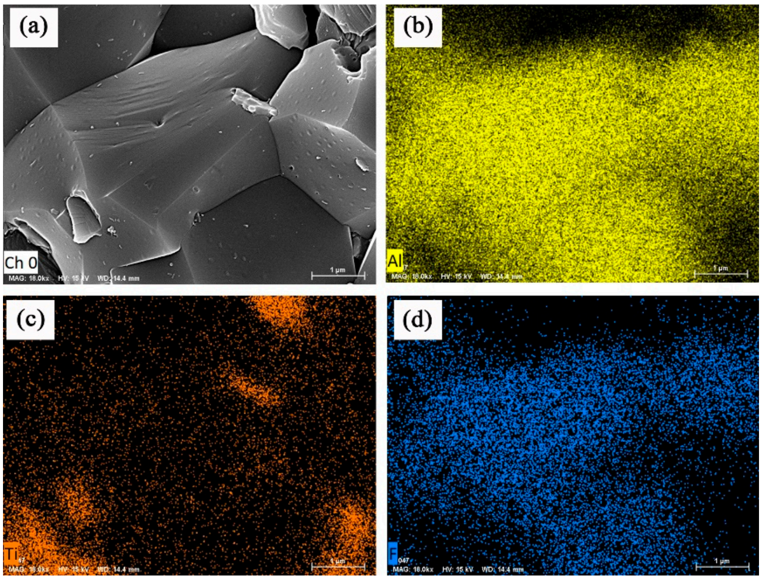

Figure 5. SEM micrograph and EDS spectra of fracture surfaces of Al_2O_3/TiC/CaF_2 self-lubricating ceramic composites: (**a**) fracture morphology of Al_2O_3/TiC/CaF_2 ceramic composites (**b**) Al element (**c**) Ti element (**d**) F element.

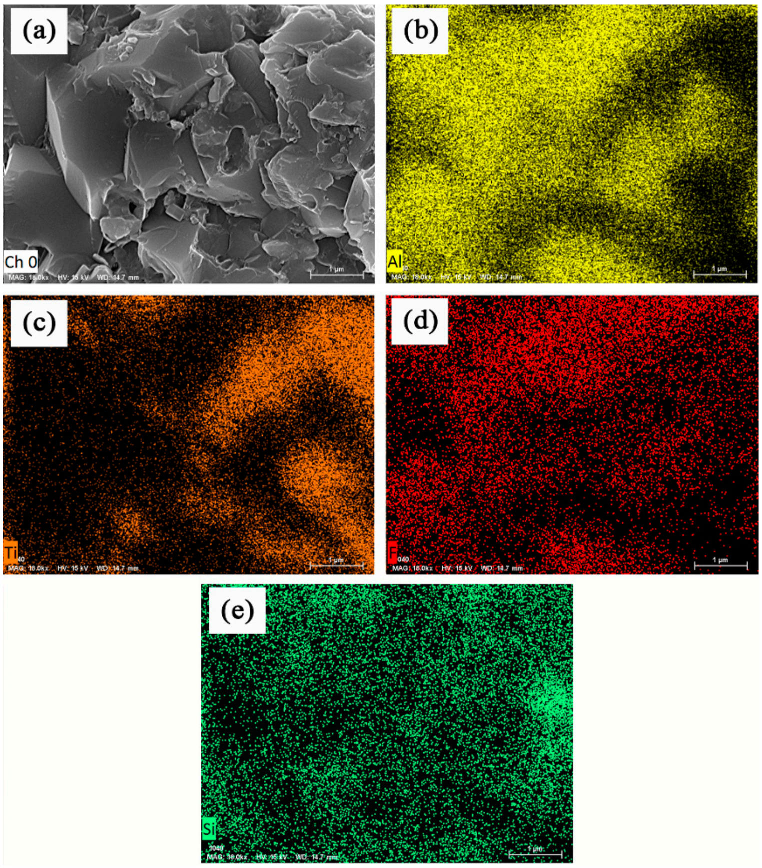

Figure 6. SEM micrograph and EDS spectra of fracture surfaces of Al_2O_3/TiC/CaF_2@SiO_2 self-lubricating ceramic composites: (**a**) fracture morphology of Al_2O_3/TiC/CaF_2@SiO_2 ceramic composites (**b**) Al element (**c**) Ti element (**d**) F element (**e**) Si element.

Table 1 shows the mechanical properties of ceramic tools with CaF_2 nanoparticles and CaF_2@SiO_2-coated nanoparticles. Compared with the ceramic tool with CaF_2 nanoparticles, the ceramic tool with CaF_2@SiO_2-coated nanoparticles had a hardness increase of 4.88%, a flexural strength increase of 17.57%, a fracture toughness increase of 12.67%. The flexural strength of the ceramic tool was also greatly improved, which was due to the change of the main fracture mode in the ceramic tool material; the hardness and fracture toughness of the ceramic tool were also improved. The addition of CaF_2@SiO_2-coated nanoparticles greatly improved the antifriction and wear resistance of the ceramic tool material; the antifriction and wear resistance of the tool material were balanced.

Table 1. Mechanical properties of the ceramic tool material.

Material	Flexural Strength/MPa	Fracture Toughness/MPa·m$^{1/2}$	Hardness/GPa
ATC	478 ± 21	4.89 ± 0.13	14.55 ± 0.19
ATCS	562 ± 23	5.51 ± 0.21	15.26 ± 0.16

4. Conclusions

In this paper, SiO_2 was successfully coated on the surface of CaF_2 nanoparticles to prepare a nano-powder with a core–shell structure. After adding CaF_2 nanoparticles and CaF_2@SiO_2-coated nanoparticles into an Al_2O_3/TiC ceramic matrix, the mechanical properties and the micro-morphology of ceramic tools were analyzed. The effects of adding CaF_2@SiO_2-coated nanoparticles on the micro-morphology and mechanical properties of the ceramic tools were compared with those of adding CaF_2 nanoparticles. The following conclusions were obtained.

1. SiO_2 shells with different thicknesses could be obtained by changing the amount of TEOS added, and the thickness of the SiO_2 shell could be controlled between 1.5 and 15 nm. However, when the TEOS amount was too large, agglomeration occurred, whereas when the TEOS amount was 3 mL, the best coating effect was obtained.
2. The ceramic tool had the best mechanical properties when CaF_2@SiO_2-coated nanoparticles were added. The flexural strength, the fracture toughness, and the hardness were 562 ± 28 MPa, 5.51 ± 0.26 MPa·m$^{1/2}$ and 15.26 ± 0.16 GPa, respectively. Compared with the ceramic tool with the CaF_2 nanoparticles, the above performances were increased by 17.57%, 12.67% and 4.88%, respectively.
3. Compared with the ceramic tool with CaF_2 nanoparticles, the ceramic tool with CaF_2@SiO_2-coated nanoparticles showed a great change in its microscopic morphology. The addition of the coated powder played a role in refining the crystal grains of the ceramic tool and, at the same time, increased its transgranular fracture, improving its performance.

Author Contributions: N.G. and Z.C. conceived and designed the experiments; N.G. performed the experiments; N.G., C.X., Z.C., and L.J. analyzed the data; N.G. and Z.C. wrote the paper.

Funding: This work was supported by Key R & D project of Shandong Province (grant number: 2019GGX104084), the National Natural Science Foundation of China (grant number: 51575285), Project for the Innovation Team of Universities and Institutes in Jinan (grant number: 2018GXRC005) and the Natural Science Foundation of Shandong Province (grant number: ZR2017LEE014).

Acknowledgments: Thanks to the co-authors of this paper for their help, editors and reviewers for their valuable suggestions for revision, the analysis and testing center of Qilu university of technology (Shandong Academy of Sciences) for its technical support, and the institutions and individuals who have provided help to this research but are not listed here.

Conflicts of Interest: The authors declare no conflict of interest.

References

1. Zhang, C.; Liu, J.; Fan, X.; Peng, Q.; Guo, X.; Jiang, D.; Qian, X.; Su, L. Compact passive Q-switching of a diode-pumped Tm, Y: CaF_2 laser near 2 mu m. *Opt. Laser Technol.* **2018**, *103*, 89–92. [CrossRef]
2. Chen, K.; Chen, M.; Yu, Z.; Wang, Q.; Li, X.; Zhu, S.; Wang, F. Corrosion of SiO_2–B_2O_3–Al_2O_3–CaF_2-R_2O (R = Na and K) enamels with different content of ZrO_2 in H_2SO_4 and NaOH solutions. *Ceram. Int.* **2019**, *45*, 14958–14967. [CrossRef]
3. Rezvani, M.; Farahinia, L. Structure and optical band gap study of transparent oxyfluoride glass-ceramics containing CaF_2 nanocrystals. *Mater. Des.* **2015**, *88*, 252–257. [CrossRef]
4. Vishwanath, S.; Liu, X.; Rouvimov, S.; Mende, P.C.; Azcatl, A.; McDonnell, S.; Wallace, R.M.; Feenstra, R.M.; Furdyna, J.K.; Jena, D.; et al. Comprehensive structural and optical characterization of MBE grown $MoSe_2$ on graphite, CaF_2 and graphene. *2D Mater.* **2015**, *2*, 24007. [CrossRef]
5. Kwon, S.; Cho, S.-H.; Lee, J.; Kang, J.; Lee, J.-H.; Cho, S.; Nersisyan, H.H. High-temperature stability of YSZ and MSZ ceramic materials in CaF_2–MgF_2–MgO molten salt system. *J. Am. Ceram. Soc.* **2017**, *101*, 2074–2083. [CrossRef]
6. Yang, Y.; Li, W.; Mei, B.; Song, J.; Yi, G.; Zhou, Z.; Liu, J. Synthesis and enhanced upconversion luminescence upon two-wavelength excitation of Er^{3+}: CaF_2 transparent ceramics. *J. Lumin.* **2019**, *213*, 504–509. [CrossRef]
7. Nakamura, F.; Kato, T.; Okada, G.; Kawaguchi, N.; Fukuda, K.; Yanagida, T. Scintillation and dosimeter properties of CaF_2 transparent ceramic doped with Eu^{2+}. *Ceram. Int.* **2017**, *43*, 604–609. [CrossRef]
8. Nakamura, F.; Kato, T.; Okada, G.; Kawaguchi, N.; Fukuda, K.; Yanagida, T. Scintillation and dosimeter properties of CaF_2 translucent ceramic produced by SPS. *J. Eur. Ceram. Soc.* **2017**, *37*, 1707–1711. [CrossRef]
9. Liu, X.; Di, W.; Qin, W. Cooperative luminescence mediated near infrared photocatalysis of CaF_2: Yb@$BiVO_4$ composites. *Appl. Catal. B Environ.* **2017**, *205*, 158–164. [CrossRef]
10. Mrityunjay, D.; Mahantayya, M.; Ramesh, M.R. Microstructure and tribological behavior of plasma sprayed NiCrAlY/WC-Co/cenosphere/solid lubricants composite coatings. *Surf. Coat. Technol.* **2018**, *354*, 92–100.
11. Gajrani, K.K.; Suvin, P.S.; Kailas, S.V.; Mamilla, R.S. Thermal, Rheological, Wettability and Hard Machining Performance of MoS_2 and CaF_2 based Minimum Quantity Hybrid Nano-Green Cutting Fluids. *J. Mater. Process. Technol.* **2019**, *266*, 25–139. [CrossRef]
12. Zhen, J.; Li, F.; Zhu, S.; Ma, J.; Qiao, Z.; Liu, W.; Yang, J. Friction and wear behavior of nickel-alloy-based high temperature self-lubricating composites against Si_3N_4 and Inconel 718. *Tribol. Int.* **2014**, *75*, 1–9. [CrossRef]
13. Yuan, J.; Zhu, Y.; Ji, H.; Zheng, X.; Ruan, Q.; Niu, Y.; Liu, Z.; Zeng, Y. Microstructures and tribological properties of plasma sprayed WC–Co–Cu–BaF_2/CaF_2 self-lubricating wear resistant coatings. *Appl. Surf. Sci.* **2010**, *256*, 4938–4944. [CrossRef]
14. Cheng, J.; Zhen, J.; Zhu, S.; Yang, J.; Ma, J.; Li, W.; Liu, W. Friction and wear behavior of Ni-based solid-lubricating composites at high temperature in a vacuum environment. *Mater. Des.* **2017**, *122*, 405–413. [CrossRef]
15. Fang, Y.; Fan, H.; Song, J.; Zhang, Y.; Hu, L. Surface engineering design of Al_2O_3/Mo self-lubricating structural ceramics—Part II: Continuous lubrication effects of a three-dimensional lubricating layer at temperatures from 25 to 800 °C. *Wear* **2016**, *360*, 97–103. [CrossRef]
16. Yang, X.; Wang, Z.; Song, P.; Wang, S.; Wang, Y.; Mao, K. Laminated structure optimization and drawing performance of Al_2O_3–TiC/Al_2O_3–TiC–CaF_2 self-lubricating laminated ceramic conical die. *Ceram. Int.* **2015**, *41*, 12480–12489. [CrossRef]
17. Wu, G.; Xu, C.; Xiao, G.; Yi, M.; Chen, Z. Structure design of Al_2O_3/TiC/CaF_2 multicomponent gradient self-lubricating ceramic composite and its tribological behaviors. *Ceram. Int.* **2018**, *44*, 5550–5563. [CrossRef]
18. Xu, C.; Xiao, G.; Zhang, Y.; Fang, B. Finite element design and fabrication of Al_2O_3/TiC/ CaF_2 gradient self-lubricating ceramic tool material. *Ceram. Int.* **2014**, *40*, 10971–10983. [CrossRef]
19. Xu, C.; Wu, G.; Xiao, G.; Fang, B. Al_2O_3/(W,Ti)C/ CaF_2 multi-component graded self-lubricating ceramic cutting tool material. *Int. J. Refract. Met. Hard Mater.* **2014**, *45*, 125–129. [CrossRef]
20. Yang, X.; Wang, Z.; Song, P.; Cheng, J.; Gu, J.; Ma, T. Dry Sliding Wear Behavior of Al_2O_3-TiC Ceramic Composites Added with Solid Lubricant CaF_2 by Cold Pressing and Sintering. *Tribol. Trans.* **2014**, *58*, 231–239. [CrossRef]
21. Kong, L.; Bi, Q.; Niu, M.; Zhu, S.; Yang, J.; Liu, W. High-temperature tribological behavior of ZrO_2–MoS_2–CaF_2 self-lubricating composites. *J. Eur. Ceram. Soc.* **2013**, *33*, 51–59. [CrossRef]

22. Chen, G.; Shen, J.; Ohulchanskyy, T.Y.; Patel, N.J.; Kutikov, A.; Li, Z.; Song, J.; Pandey, R.K.; Ågren, H.; Prasad, P.N.; et al. (α-$NaYbF_4$:Tm^{3+})/CaF_2 Core/Shell Nanoparticles with Efficient Near-Infrared to Near-Infrared Upconversion for High-Contrast Deep Tissue Bioimaging. *ACS Nano* **2012**, *6*, 8280–8287. [CrossRef] [PubMed]
23. Mahn, S.; Kemnitz, E. Modification of low-molecular polylactic acid by CaF_2 nanoparticles: A new approach to change its material properties. *J. Appl. Polym. Sci.* **2019**, *136*, 47875. [CrossRef]
24. Cortelletti, P.; Facciotti, C.; Cantarelli, I.X.; Canton, P.; Quintanilla, M.; Vetrone, F.; Speghinia, A.; Pedronia, M. Nd^{3+} activated CaF_2 NPs as colloidal nanothermometers in the biological window. *Opt. Mater.* **2017**, *68*, 29–34. [CrossRef]
25. Cui, X.; Hu, T.; Wang, J.; Zhong, X.; Chen, Y.; Zhang, J.; Li, X.; Yang, J.; Gao, C. Effect of Tb-doped Concentration Variation on the Electrical and Dielectric Properties of CaF_2 Nanoparticles. *Nanomaterial* **2018**, *8*, 532. [CrossRef]
26. Meza, L.R.; Das, S.; Greer, J.R. Strong, lightweight, and recoverable three-dimensional ceramic nanolattices. *Science* **2014**, *345*, 1322–1326. [CrossRef]
27. Yang, H.; Ye, F.; Liu, Q.; Liu, S.; Gao, Y.; Liu, L. A novel silica aerogel/porous Si_3N_4 composite prepared by freeze casting and sol-gel impregnation with high-performance thermal insulation and wave-transparent. *Mater. Lett.* **2015**, *138*, 135–138. [CrossRef]
28. Zhang, J.; Xiao, G.; Zhang, J.; Yi, M.; Chen, Z.; Zhang, W.; Xu, C. Al_2O_3/WB_2 composite ceramic tool material reinforced with graphene oxide. *Int. J. Refract. Met. Hard Mater.* **2019**, *81*, 173–182. [CrossRef]
29. Singh, S.; Meena, V.K.; Sharma, M.; Singh, H. Preparation and coating of nano-ceramic on orthopaedic implant material using electrostatic spray deposition. *Mater. Des.* **2015**, *88*, 278–286. [CrossRef]
30. Sun, S.; Xu, Q. Fabricating a Novel Intragranular Microstructure for Al_2O_3/$GdAlO_3$ Ceramic Composites. *Material* **2018**, *11*, 1879. [CrossRef]
31. Dubey, M.K.; Bijwe, J.; Ramakumar, S.S.V. Effect of dispersant on nano-PTFE based lubricants on tribo-performance in fretting wear mode. *RSC Adv.* **2016**, *6*, 22604–22614. [CrossRef]
32. Casati, R.; Vedani, M. Metal Matrix Composites Reinforced by Nano-Particles—A Review. *Metals* **2014**, *4*, 65–83. [CrossRef]
33. Mirjavadi, S.S.; Alipour, M.; Emamian, S.; Kord, S.; Hamouda, A.M.S.; Koppad, P.G.; Keshavamurthy, R. Influence of TiO_2 nanoparticles incorporation to friction stir welded 5083 aluminum alloy on the microstructure, mechanical properties and wear resistance. *J. Alloy. Compd.* **2017**, *712*, 795–803. [CrossRef]
34. Dambatta, Y.S.; Sayuti, M.; Sarhan, A.A.D.; Hamdi, M. Comparative study on the performance of the MQL nanolubricant and conventional flood lubrication techniques during grinding of Si_3N_4 ceramic. *Int. J. Adv. Manuf. Technol.* **2018**, *96*, 3959–3976. [CrossRef]
35. Vijayakumar, S.; Vadivel, S. Fiber optic ethanol gas sensor based WO_3 and WO_3/gC_3N_4 nanocomposites by a novel microwave technique. *Opt. Laser Technol.* **2019**, *118*, 44–51. [CrossRef]
36. Wang, H.; Ma, R.; Nienhaus, K.; Nienhaus, G.U. Formation of a Monolayer Protein Corona around Polystyrene Nanoparticles and Implications for Nanoparticle Agglomeration. *Small* **2019**, *15*, e1900974. [CrossRef]
37. Chen, H.; Xu, C.; Xiao, G.; Chen, Z.; Ma, J.; Wu, G. Synthesis of (h-BN)/SiO_2 core–shell powder for improved self-lubricating ceramic composites. *Ceram. Int.* **2016**, *42*, 5504–5511. [CrossRef]
38. Song, C.; Chen, J.; Abell, J.L.; Cui, Y.; Zhao, Y. Ag-SiO_2 Core-Shell Nanorod Arrays: Morphological, Optical, SERS, and Wetting Properties. *Langmuir* **2012**, *28*, 1488–1495. [CrossRef]
39. Hu, Y.; Xu, C.; Xiao, G.; Yi, M.; Chen, Z.; Zhang, J. Electrostatic self-assembly preparation of reduced graphene oxide-encapsulated alumina nanoparticles with enhanced mechanical properties of alumina nanocomposites. *J. Eur. Ceram. Soc.* **2018**, *38*, 5122–5133. [CrossRef]
40. He, J.; Zheng, W.; Ligmajer, F.; Chan, C.F.; Bao, Z.; Wong, K.L.; Chen, X.; Hao, J.; Dai, J.; Yu, S.F.; et al. Plasmonic enhancement and polarization dependence of nonlinear upconversion emissions from single gold nanorod@SiO_2@CaF_2:Yb^{3+}, Er^{3+} hybrid core-shell-satellite nanostructures. *Light Sci. Appl.* **2017**, *6*, e16217. [CrossRef]
41. Hu, D.; Zhao, F.; Zhang, Z.; Miao, L.; Ma, R.; Zhao, W.; Ren, L.; Zhang, G.; Zhai, L.; Wang, D.; et al. Synthesis and magnetic properties of monodisperse $CoFe_2O_4$ nanoparticles coated by SiO_2. *Ceram. Int.* **2018**, *44*, 22462–22466. [CrossRef]

42. Wu, G.; Xu, C.; Xiao, G.; Yi, M.; Chen, Z.; Chen, H. An advanced self-lubricating ceramic composite with the addition of core-shell structured h-BN@Ni powders. *Int. J. Refract. Met. Hard Mater.* **2018**, *72*, 276–285. [CrossRef]
43. Zhang, L.; Ren, Y.; Peng, S.; Guo, D.; Wen, S.; Luo, J.; Xie, G. Core-shell nanospheres to achieve ultralow friction polymer nanocomposites with superior mechanical properties. *Nanoscale* **2019**, *11*, 8237–8246. [CrossRef] [PubMed]
44. Jia, C.; Dai, Y.; Yang, Y.; Chew, J.W. Nickel-cobalt catalyst supported on TiO_2-coated SiO_2 spheres for CO_2 methanation in a fluidized bed. *Int. J. Hydrog. Energy* **2019**, *44*, 13443–13455. [CrossRef]
45. Chen, Z.; Guo, N.; Ji, L.; Guo, R. An advanced self-lubricating ceramic composite with the addition of core-shell structured CaF_2@Al_2O_3 powders. *Int. J. Appl. Ceram. Technol.* **2019**, *16*, 753–760. [CrossRef]